NANO MICRO
small

Supporting Information

for *Small,* DOI: 10.1002/smll.201803342

Patterned Optoelectronic Tweezers: A New Scheme for Selecting, Moving, and Storing Dielectric Particles and Cells

*Shuailong Zhang, Nika Shakiba, Yujie Chen, Yanfeng Zhang, Pengfei Tian, Jastaranpreet Singh, M. Dean Chamberlain, Monika Satkauskas, Andrew G. Flood, Nazir P. Kherani, Siyuan Yu, Peter W. Zandstra, and Aaron R. Wheeler**

Supporting Information for

Patterned Optoelectronic Tweezers: A New Scheme for Selecting, Moving, and Storing Dielectric Particles and Cells

Shuailong Zhang[1,2,3], Nika Shakiba[3], Yujie Chen[4], Yanfeng Zhang[4], Pengfei Tian[5], Jastaranpreet Singh[3], M. Dean Chamberlain[1,2], Monika Satkauskas[1,2], Andrew G. Flood[6], Nazir P. Kherani[6,7], Siyuan Yu[4,8], Peter W. Zandstra[1,3,9,10,11] and Aaron R. Wheeler[1,2,3,*]

1. *Donnelly Centre for Cellular and Biomolecular Research, University of Toronto, Toronto, ON, Canada M5S 3E1*
2. *Department of Chemistry, University of Toronto, Toronto, ON, Canada M5S 3H6*
3. *Institute for Biomaterials and Biomedical Engineering, University of Toronto, Toronto, ON, Canada M5S 3G9*
4. *State Key Laboratory of Optoelectronic Materials and Technologies, School of Electronics and Information Technology, Sun Yat-sen University, Guangzhou 510275, China*
5. *Institute for Electric Light Sources, Fudan University, Shanghai, 200433, China*
6. *Department of Electrical and Computer Engineering, University of Toronto, Toronto, ON, Canada M5S 3G4*
7. *Department of Materials Science and Engineering, University of Toronto, Toronto, ON, Canada M5S 3E4*
8. *Photonics Group, Merchant Venturers School of Engineering, University of Bristol, Bristol BS81UB, United Kingdom*
9. *Medicine by Design, University of Toronto, Toronto, ON, Canada M5S 3G9*
10. *School of Biomedical Engineering, University of British Columbia, Vancouver, BC, Canada V6T 1Z3*
11. *Michael Smith Laboratories, University of British Columbia, Vancouver, BC, Canada V6T 1Z3*

Correspondence: Aaron R. Wheeler, Email: aaron.wheeler@utoronto.ca

S1. Assembly of p-OET Device

Figure S1 shows images of p-OET bottom and top plates before and after assembly.

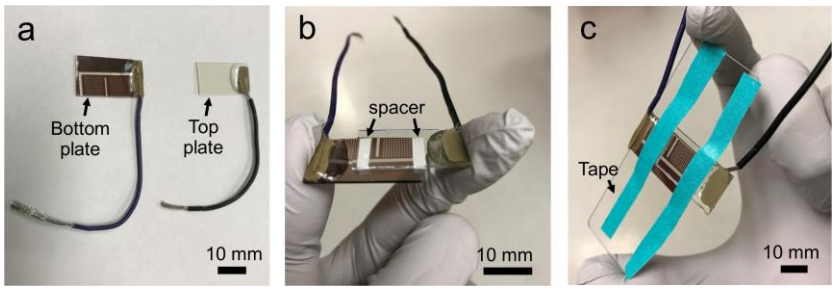

Figure S1. p-OET device assembly. (a) Picture of bottom and top plates of a p-OET device. (b) Picture of an assembled device, with the two plates held together by a 150-µm-thick spacer. (c) Picture of a p-OET device affixed to the top of a microscope slide with tape.

S2. Light-induced heating

To study light-induced heating, a square-shaped light pattern was projected onto the photoconductive layer of an OET device (without patterned photoconductive layer) filled with buffer. The optical power was measured by a power-meter and the optical power density was calculated for each objective used, shown in Figure S2a (black histogram). As shown, the optical power density increases as the magnification increases, with the maximum power density measured to be 2.5 W/cm^2 for the 20x objective. Figure S2a (red histogram) shows the

temperature profile of the illuminated region on the photoconductive layer, measured using a high-resolution infrared camera. As shown, the temperature measured for each of the illuminated conditions is greater than that for a "dark" control by ~2-4°C. A two-tailed t-test (two sample unequal variance) indicates statistical difference between the temperature measured for each illuminated condition relative to the "dark" control (2.5x objective and "dark" control: $p=1.2\times10^{-7}$; 5x objective and "dark" control: $p=1.2\times10^{-8}$; 10x objective and "dark" control: $p=3.7\times10^{-7}$; 20x objective and "dark" control: $p=1.8\times10^{-5}$).

The heating effect described above (a few °C) may seem modest, but in fact can be problematic when applied for extended periods to small volumes of fluid. Fluid volumes in the OET chamber were tracked by following the air-liquid boundary in microscope images; as time progressed, the area covered by liquid (readily converted to volume, knowning the dimensions of the OET chamber) became smaller as consequence of evaporation. Figure S2b shows the volumes measured before and after 25 minutes incubation while being illuminated (or not) by the square-shaped light pattern. 15 μL medium was first pipetted into a p-OET device. A two-tailed t-test (two sample unequal variance) indicates statistical difference between the fluid volumes for each illuminated condition relative to the "dark" control (10x objective and "dark" control: $p=4.7\times10^{-4}$; 20x objective and "dark" control: $p=9\times10^{-4}$). Figure S2c shows more detail for the 10x objective case (which was used for all experiments described in the main text), illustrating how the illuminated condition diverges from the dark condition after only a few minutes of incubation.

The amount of light-induced evaporation indicated in Fig. S2b-c is substantial, and can change many properties of the liquid medium, including conductivity, osmolarity and viscosity. In addition, this level of evaporation can induce undesired fluidic shear force that causes trapped micro-objects to move. This effect motivated the development of p-OET, which allows efficient manipulation of micro-objects with light but also preservation of the micro-objects in targeted areas without light, minimizing the light-induced heating and evaporation.

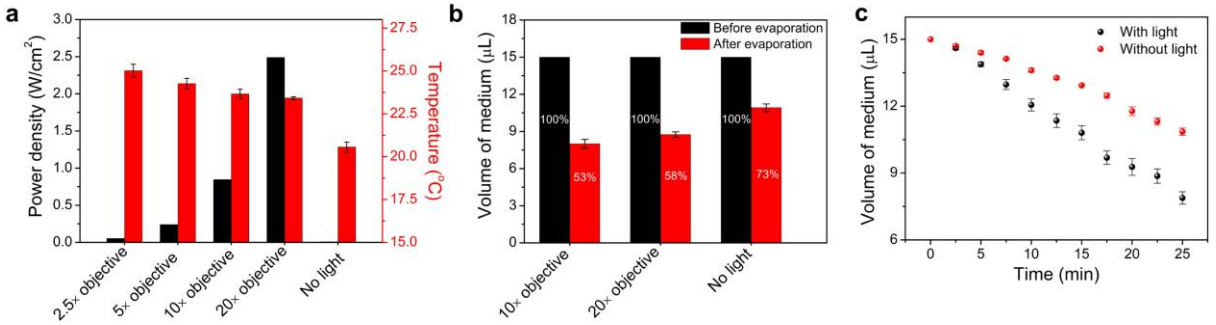

Figure S2. Light-induced heating in OET. (a) Optical power density (black, left axis) and temperature (red, right axis) measured after 3 min of illumination with a square light pattern projected onto an OET device through 2.5x, 5x, 10x, or 20x microscope objectives (or with no illumination). (b) Liquid volume in the chamber before (black) and after 25 minutes incubation (red) in an OET device illuminated by a sqare light pattern projected onto an OET device through 10x or 20x microscope objectives (or with no illumination). (c) Time-dependent change of liquid volume with (black) and without (red) continuous illumination through a 10x objective. Error bars for all data represent ± 1 std. dev. from n = 5 measurements per condition.

S3. OET Trap Profile

As an optical micromanipulation tool, it is important to characterize the effectiveness of OET to manipulate targeted objects in terms of trap profile and imposed DEP force. The OET-fluid system reported here operates in the laminar flow regime (Reynolds number: Re << 1), in which the DEP force responsible for bead/cell motion is approximately equivalent to the viscous drag force, which is given by Stoke's law [1-4]:

$$F_{DEP} = F_{drag} \quad (1)$$

$$F_{drag} = 6\pi\eta r v \quad (2)$$

where η is the fluid viscosity, r is the radius of the bead/cell, and v is travelling velocity. Since in this system the beads/cells are forced to sit in proximity of the device surface due to gravity, Faxen's correction was used to adjust the calculations of viscous drag force and DEP force based on the radius of each object.[1-5]

A 'doughnut'-shaped OET trap is described in the main text (see Figure 3a,b and Movie S1). To study the force-profile for a 25-µm diameter polystyrene bead trapped in the doughnut-shaped trap, the motorized stage velocity was gradually increased until the bead no longer followed the light pattern (and fell out of the trap). By measuring the center-to-center displacement between the bead and the light pattern at different velocities, a trap profile can be plotted for the bead. Figure S3a,b shows the measured displacement D_o (discrete points) for a 25-µm-diameter bead manipulated by the doughnut-shaped light pattern at 7 $V_{p\text{-}p}$ and 20 $V_{p\text{-}p}$, respectively. Experimental data were compared with simulated trap profiles (solid lines) as described below. As shown, beads in the center of the trap experienced lowest force, and experienced larger forces as they moved closer to the inner-edge of the doughnut (before escaping the trap). The simulation also predicts a similar set of forces at the outer-edge of the trap.

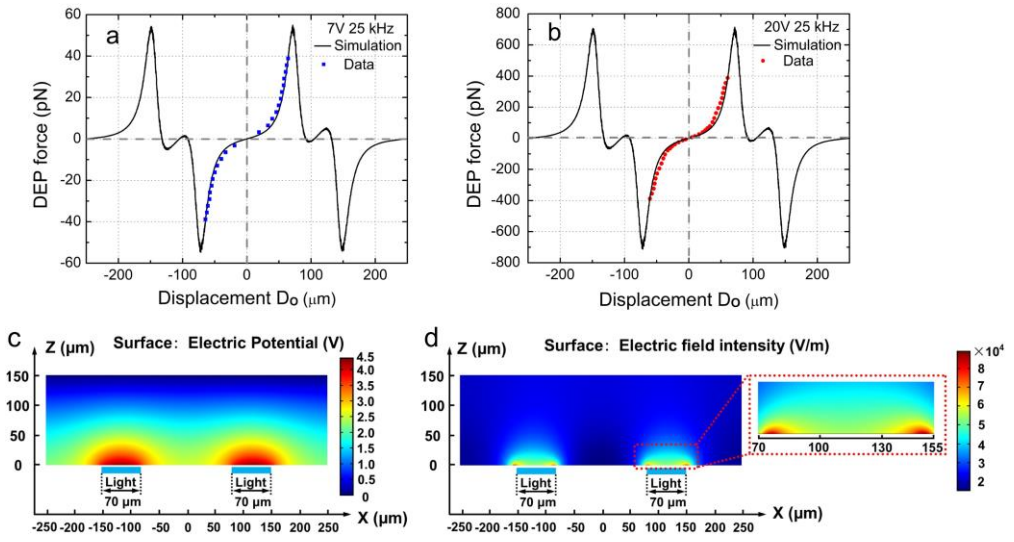

Figure S3. Trap profiles for a 25-µm-diameter polystyrene bead in a doughnut-shaped OET trap. (a-b) Measured bead-displacements (blue squares and red circles) and simulated trap profiles (solid lines, see text below) for a bead in the trap moved at different velocities. The OET device is driven at an AC potential of (a) 7 $V_{p\text{-}p}$ and (b) 20 $V_{p\text{-}p}$, respectively. Simulated distributions of (c) electric potential and (d) electric field in X-Z cross-sectional slices through the center of the doughnut-shaped trap at 7 $V_{p\text{-}p}$, with heat maps from low (blue) to high (red) potential and field, respectively. The inset in (d) shows a magnified region around one side of the doughnut.

Two dimensional (2D) simulations of the XZ cross-sections of doughnut-shaped OET traps were generated in COMSOL Multiphysics using the AC/DC module (COMSOL Inc., Burlington, MA, accessed via license obtained through CMC Microsystems, Kingston, Canada). The AC/DC module uses the quasi-static approximation which assumes that the wavelength of applied AC signal is much larger than the dimensions of the simulation model. This assumption is justified for the model shown in Figure S3, as the wavelength of the applied AC signal is 6×10^3 m, while the critical lengths evaluated in the model are 500 μm across X plane and 150 μm across Z plane. The boundary conditions were set to perfect electrical insulation at the sides and continuity for all interior boundaries. The top boundary was set to 0 V and the bottom boundary was set to 7 $V_{p\text{-}p}$ or 20 $V_{p\text{-}p}$ to simulate the applied AC signal (frequency set to 25 kHz). The model included a 1-μm-thick a-Si:H layer at the bottom and a 149-μm-thick liquid chamber. The conductivities σ and permittivities ε were set to $\sigma_{silicon\text{-}light} = 1\times10^{-4}$ S/m, $\sigma_{silicon\text{-}dark} = 1\times10^{-6}$ S/m, $\varepsilon_{silicon} = 11.7$, $\sigma_{medium} = 5\times10^{-3}$ S/m, and $\varepsilon_{medium} = 80$. The model employed a free triangular mesh with a maximum element size of 5 μm, a minimum element size of 0.004 μm, a maximum element growth rate of 1.02, a curvature factor of 0.05, and a resolution of narrow regions of 5.

The conditions described here are similar to those of a well-developed model for a doughnut-shaped OET trap.[1,2,4-6] Figure S3c illustrates the simulated electric potential distribution; as shown, there is a large electric potential variation along Z-axis (from the liquid medium to the bottom surface) in the region illuminated with light relative to that without, caused by the light-induced conductivity change in the a-Si:H. This effect also induces a large electric potential variation along X-axis at the boundary regions between the dark and illuminated region above the a-Si:H layer. Figure S3d shows the simulated electric field distribution in the OET device. As indicated, there exist strong electric fields and field variations (field gradients) at the boundaries of the illuminated regions, resulting in strong DEP force at the edge of the light pattern as observed in the experiments. Based on classic DEP theory and a widely-used dipole approximation method,[1,3,6,7] the force acting on a polystyrene micro-bead is expressed as:

$$F_{DEP} = 2\pi r^3 \varepsilon_m Re[K(\omega)]\nabla E^2 \qquad (3)$$

where r is the radius of the bead, ε_m is the permittivity of the media, $\mathrm{Re}[K(\omega)]$ is the real component of the Clausius-Mossotti (CM) factor (which is dependent on angular frequency of the applied field ω), and ∇E^2 is the gradient of the square of the electric field. By applying the models of electric potential and electric field (Figure S3c,d) at different bead-displacements within the trap, the trap force-profiles can be simulated, shown in Figure S3a,b (solid lines).

In the simulations described above, the gradient of the electric field's square (∇E^2) was simulated along the X axis for a 25-μm-diameter bead touching the a-Si:H surface (i.e., the Z-dimension of the bead center is 12.5 μm above the a-Si:H surface), with the real component of the CM factor of -0.5. The simulated ∇E^2 for the center of the bead was used to calculate the DEP force imposed on the bead; that is, the bead was simplified to point dipole. This is imperfect, as the actual DEP force varies over the volume of the bead, and in addition, the bead may experience greater frictional forces in OET device (including electrostatic interactions with the surface), which are not accounted for in the point-dipole model. Nevertheless, after scaling the simulation results by a factor of 1.7 in Figure S3a and a factor of 2.9 in Figure S3b, there is a qualitative match between the simulated

results (solid lines) and measured results (blue squares and red circles).

S4. p-OET Simulations

COMSOL Multiphysics was also used to develop two models for p-OET applications, including the system described in Figure 3 and Figure 4 in the main text. The boundary conditions were identical to those listed above, and the quasi-static approximation is justified for these models, as the critical dimensions are 400 μm across the X plane and 150 μm across the Z plane (for Figure 3), and 500 μm across X and Y planes, and 150 μm across Z plane (for Figure 4).

Like the OET model described above, the p-OET model used in Figure 3 in the main text is a 2D XZ cross-section of a device. In this case, the device bears a 200-nm-thick ITO layer, a 1-μm-thick micro-patterned a-Si:H layer and a 148.8-μm-thick liquid chamber. The conductivities σ and permittivities ε were set to σ_{ITO} =5×10^5 S/m, ε_{ITO} = 4, $\sigma_{silicon}$ =1×10^{-6} S/m, $\varepsilon_{silicon}$ = 11.7, σ_{medium} =5×10^{-3} S/m, and ε_{medium} =80. The mesh was identical to the one described for OET, above. Likewise, the model was applied to a 25-μm-diameter polystyrene bead as a point-dipole approximation (as above) and fitted to the data after scaling by a factor of 3.6 in Figure 3e, a factor of 5.1 in Figure 3f.

The model used in Figure 4 in the main text is a three-dimensional (3D) simulation of a p-OET device with a micro-patterned a-Si:H layer. This model includes a 200-nm-thick ITO layer, a 1-μm-thick micro-patterned a-Si:H layer and a 148.8-μm-thick liquid chamber. The conductivities σ and permittivities ε were set to σ_{ITO} =5×10^5 S/m, ε_{ITO} = 4, $\sigma_{silicon}$ =1×10^{-6} S/m, $\varepsilon_{silicon}$ = 11.7, σ_{medium} =5×10^{-3} S/m, and ε_{medium} =80. The model employed a free tehrahedral mesh with a maximum element size of 20 μm, a minimum element size of 0.1 μm, a maximum element growth rate of 1.35, a curvature factor of 0.4, and a resolution of narrow regions of 0.85.

S5. OET manipulation of cells

MCF-7 human breast cancer cells (labelled in green) and ARPE-19 human retinal pigment epithelial cells (labelled in red) were manipulated by light patterns in OET device. As shown in Figure S4a,b, an MCF-7 breast cancer cell and an ARPE-19 human retinal pigment epithelial cell were isolated in separate doughnut-shaped OET traps and then were brought into contact by moving and merging the two traps together, using time-varying optical animations (see Movie S5 for more details). Shown in Figure S4c,d are microscope images of a group of MCF-7 cells and ARPE-19 cells before and after being forced together by shrinking a OET trap by reducing the radius of a doughnut-shaped light pattern (see Movie S5 for more details).

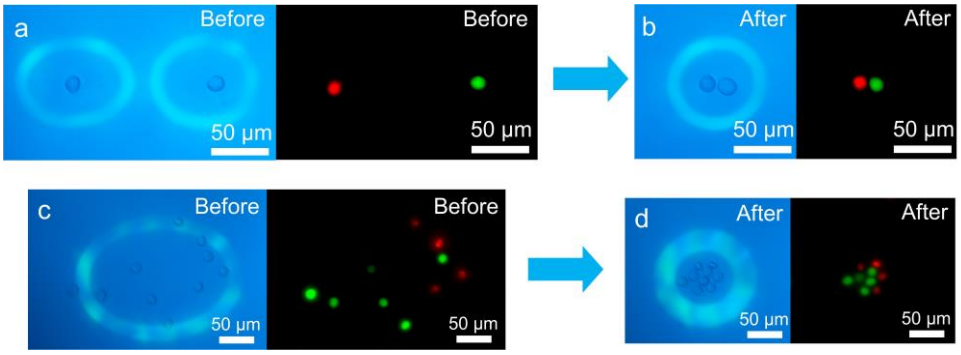

Figure S4. Manipulation of MCF-7 human breast cancer cells (pre-labelled green by CellTracker dye) and ARPE-19 human retinal pigment epithelial cells (pre-labelled red by CellTracker dye) by OET. (a) Bright-field (left) and fluorescent microscope image (right) showing an MCF-7 cell and an ARPE-19 cell positioned in two doughnut-shaped OET traps. (b) Bright-field (left) and fluorescent microscope image (right) showing the MCF-7 cell and ARPE cell after moving the two traps together. (c) Bright-field (left) and fluorescent microscope image (right) showing a group of MCF-7 cells and ARPE-19 cells before manipulation. (d) Bright-field (left) and fluorescent microscope image (right) showing MCF-7 cells and ARPE-19 cells after shrinking the OET trap to push them together. Devices in these experiments were driven at 7 $V_{p\text{-}p}$ at 25 kHz. Additional examples of cell manipulation by OET can be found in Movie S5 in the Supporting Information.

S6. Supplementary Movies:

Movie S1: A 25-µm-diameter polystyrene bead was immobilized in a stationary OET doughnut-trap, and made to move by translating the microscope stage at 10 µm/s (clip 1) and 60 µm/s (clip 2). The device was operated at an AC bias of 7 $V_{p\text{-}p}$ at 25 kHz.

Movie S2: A 25-µm-diameter polystyrene bead was immobilized in a stationary OET doughnut-trap, and was then made to move toward a p-OET feature (an exposed ITO/a-Si:H boundary) by translating the microscope stage at 2 µm/s. Eventually the bead came too close to the p-OET feature and it escaped into the fluid in the Z-dimension. The device was operated at an AC bias of 7 $V_{p\text{-}p}$ at 25 kHz.

Movie S3: 15-µm-diameter polystyrene beads were repelled by a stationary OET rectangle, and then were made to move toward a p-OET feature (an exposed ITO/a-Si:H boundary in clip 1, and the edge of a p-OET trap in clip 2) by translating the microscope stage. Eventually the beads came too close to the p-OET features and they escaped into the fluid in the Z-dimension. The devices were operated at an AC bias of 7 $V_{p\text{-}p}$ at 25 kHz.

Movie S4: 15-µm-diameter polystyrene beads were immobilized (one-by-one) in a stationary OET doughnut-trap, and then were made to move (one-by-one) onto a p-OET trap along patterned a-Si:H tracks by translating the microscope stage. The devices were operated at an AC bias of 20 $V_{p\text{-}p}$ at 25 kHz.

Movie S5: MCF-7 cells and ARPE-19 cells were manipulated by moving and shrinking OET patterns (clip 1) or shrinking an OET pattern (clip 2) projected onto a stationary microscope stage. The devices were operated at an AC bias of 7 $V_{p\text{-}p}$ at 25 kHz.

Movie S6: MCF-7 cells and ARPE-19 cells were immobilized (on-by-one) in a stationary OET doughnut-trap, and then were made to move (one-by-one) onto a p-OET trap along a patterned a-Si:H track by translating the microscope stage. The OET doughnut-trap design and orientation was modified as needed. The device was operated at an AC bias of 7 V_{p-p} at 25 kHz.

S7. Supporting References

1. S. L. Neale, A. T. Ohta, H. Y. Hsu, J. K. Valley, A. Jamshidi, M. C. Wu, Opt. Exp. **2009**, 17, 5231.

2. S. L. Neale, M. Mazilu, J. I. B. Wilson, K. Dholakia, T. F. Krauss, Opt. Exp. **2007**, 15, 12619.

3. S. B. Huang, M. H. Wu, Y. H. Lin, C. H. Hsieh, C. L. Yang, H. C. Lin, C. P. Tseng, G. B. Lee, Lab Chip **2013**, 13, 1371.

4. S. Zhang, J. Juvert, J. M. Cooper, S. L. Neale, Sci. Rep. **2016**, 6, 32840.

5. S. Zhang, Y. Liu, J. Juvert, P. Tian, J. C. Navarro, J. M. Cooper, S. L. Neale, Appl. Phys. Lett. **2016**, 109, 021110.

6. S. Xie, X. Wang, N. Jiao, S. Tung, L. Liu, Lab Chip **2017**, 17, 2046.

7. R. Pethig, Biomicrofluidics **2010**, 4, 022811.